

Complete matched asymptotic expansions for velocity statistics in turbulent channels

Peter A. Monkewitz
 Ecole Polytechnique Fédérale de Lausanne (EPFL)
 CH-1015, Lausanne, Switzerland
 email: peter.monkewitz@epfl.ch

January 6, 2026

Complete high fidelity matched asymptotic expansions (abbreviated MAE's) are developed for the first and second order turbulence statistics in channel flow from 11 direct numerical simulations (abbreviated DNS). To put the crucial identification of overlaps on a solid footing, a simple a priori test is devised, which only requires a DNS or experimental profile and the presumed overlap of the MAE for the quantity in question.

This test fully supports the form $c_0 - c_1 Y^{1/4}$ of the overlaps for the stream-wise and cross-stream normal stresses $\langle uu \rangle$ and $\langle ww \rangle$, which has been advocated by Chen & Sreenivasan (2022, 2023, 2025) and Monkewitz (2022, 2023) and will be designated “CS” throughout the paper. The first MAE analysis of the wall-normal stress $\langle vv \rangle$ then reveals a $Re_\tau^{-5/4}$ scaling, i.e. an overlap of the form $c_0 - c_1 Y^{5/4}$, which is extensively documented.

Finally the logarithmic indicator function $\Xi = y dU/dy$ for the mean velocity profile (abbreviated MVP) is reanalyzed, with special attention devoted to its oscillatory approach to the logarithmic MVP overlap. The latter is compared to the spatial oscillations of $\langle uu \rangle$ in the concluding section, together with further observations and suggestions.

1 Introduction

The research aimed at the understanding of wall turbulence has been significantly advanced in the last 20 years by the availability of high quality DNS data, but there is still no general agreement on the Reynolds number scaling of the most basic turbulence statistics, such as turbulent stresses.

In the following, all velocities are inner scaled with the friction velocity $\hat{u}_\tau \equiv (\hat{\tau}_{\text{wall}}/\hat{\rho})^{1/2}$, where “hats” denote dimensional quantities. All lower case coordinates are inner scaled, without “+”-superscripts to simplify notation, while upper case coordinates are outer-scaled. The Reynolds number

Re_τ , finally, is the friction Reynolds number throughout the paper.

The recent efforts to understand the Reynolds number scaling of moments in wall turbulence, in particular of the normal stresses $\langle uu \rangle$ and $\langle ww \rangle$, have been dominated by two “schools” or models:

- *The “attached eddy” model with unbounded stresses*

The unbounded model has been developed from the “attached eddy hypothesis” of Townsend (1976) by Perry *et al.* (1986), Perry & Li (1990) and Perry *et al.* (1994), among others, and has been reviewed by Marusic & Monty (2019). One of its main predictions are logarithmic overlaps for some of the turbulent stresses. For $\langle uu \rangle$ Marusic *et al.* (2013) have proposed

$$\langle uu \rangle_{OL}^{\log} = 2.1 - 1.26 \ln Y \quad , \quad (1)$$

which is indicated by black dash-dotted lines in figures 1(a) and (b). Since the inner expansion of $\langle uu \rangle(y)$ has to asymptote to the overlap $[2.1 - 1.26 \ln y + 1.26 \ln \text{Re}_\tau]$, its growth with Re_τ is unlimited.

As required by MAE, the data merge at $y \approx 700$ (arrows in fig. 1a) into the presumed logarithmic overlap and follow it up to $Y \approx 0.15$, where they start to fall below the logarithm (1). It is already noted here that both LCC and Melbourne data are nicely fitted by the “CS” overlap (2) all the way to $Y \approx 0.5$, well beyond the point where the data diverge from the logarithmic fit (1). On the small- Y end, the high Reynolds number experimental data are not sufficiently reliable to decide whether they follow equation (1) or (2). Furthermore, the offset of the Superpipe data will not be discussed here, as this paper is focussed exclusively on channels.

- *The “CS” model with a finite limit for stresses as $\text{Re}_\tau \rightarrow \infty$*

In a series of recent papers, Chen & Sreenivasan (2021, 2022, 2023, 2025) have argued that the stream-wise and cross-stream normal stresses $\langle uu \rangle$ and $\langle ww \rangle$ remain bounded in the limit of $\text{Re}_\tau \rightarrow \infty$, with finite Reynolds number corrections of order $\text{Re}_\tau^{-1/4}$. The proposal has been motivated by the bounded dissipation of turbulence energy. Even though this rationale does not appear to be “watertight”, the $\text{Re}_\tau^{-1/4}$ scaling has received strong support from the data analyses of Monkewitz (2022) and Monkewitz (2023). The best fit for the “CS” overlap of the $\langle uu \rangle$ channel data used in this paper is

$$\langle uu \rangle_{OL}^{CS} = 10.6 - 10 Y^{1/4} \quad , \quad (2)$$

which is indicated by the red dotted lines in figure 1.

A masterful and extensive account of past research on the subject has been given in section 1 of Chen & Sreenivasan (2023), henceforth referred to as CS23, and the reader is referred to this paper for more background. While these authors have proposed and discussed the “CS” structure of the $\langle uu \rangle$, $\langle ww \rangle$ and $\langle pp \rangle^{1/2}$ overlaps in earlier papers, the near-perfect collapse of these quantities between wall and respective peaks, when normalized by

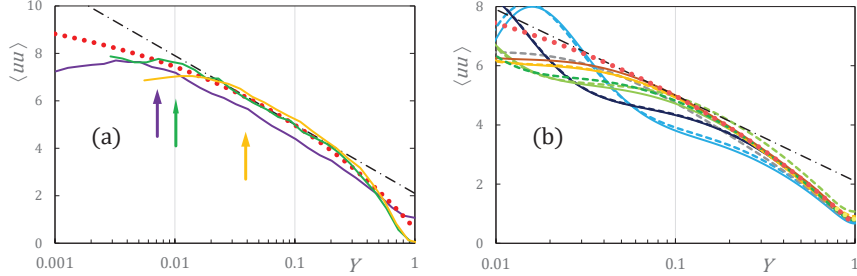


Figure 1: Streamwise normal stress $\langle uu \rangle$ versus Y . (a) Figure 1 of Marusic *et al.* (2013) replotted versus Y ; — (orange: Melbourne windtunnel; green: LCC; violet: Superpipe; SLTEST omitted); \uparrow , $y = 700$ for the three cases. —·— (black), logarithmic fit (1); ●●● (red), “bounded dissipation” overlap (2). (b) Analogue for the channel data of table 1 with addition of full outer $\langle uu \rangle_{out}$ (equ. 7 of section 3) (wake indicated by yellow ●●●) .

their peak values, demonstrated in CS23, is new. In technical MAE terms, this collapse is explained by the proportionality of f_0 and f_1 in equation (3.9) of CS23, but its important implications for the modelling of near-wall turbulent structures remain to be explored. However, no complete asymptotic expansions are given in CS23 nor in other papers - So far, the only such expansion is the one by Monkewitz (2022) for $\langle uu \rangle$.

The present paper is focussed entirely on channels, as the largest number of DNS from different sources are available for this “canonical” flow. Section 2 starts with a brief review of MAE (see e.g. Kevorkian & Cole, 1981; Wilcox, 1995, etc.), focussed on the identification of overlaps, and proposes a simple and effective diagnostic to distinguish between overlaps and mere fits of DNS profiles. Section 3 then presents new 2-term inner and 1-term outer expansions for $\langle uu \rangle$, which are significantly improved relative to Monkewitz (2022) and explicitly reveal the scales of its inner spatial oscillations. Then, the first complete inner, outer and composite expansions for $\langle ww \rangle$ and $\langle vv \rangle$ are developed in sections 4 and 5.

In section 6, a new MAE description of the log indicator function $\Xi \equiv y(dU/dy)$ for the mean velocity U is developed. The motivation for including the MVP Ξ in this paper is the first characterization of its slope oscillations, which are compared to those of $\langle uu \rangle$ in the concluding section 7. This last section also regroups a proposal for testing the scaling of $\langle vv \rangle$ and speculations on the origin of the strong flow dependence of the slope of the outer quasi-linear parts of channel, pipe and ZPG TBL MVP’s. The pressure, on the other hand, will not be discussed in this paper. Even though its overlap and near-wall collapse are rather convincing in CS23, the implications of the pressure decomposition into “rapid” and “slow” components, related to squares of perturbation velocities, and a “Stokes” component,

Table 1: Channel DNS profiles considered in the present study, with the line style/color scheme used in all figures

No.	Re_τ	Reference	line style/color
#1	944	Hoyas & Jiménez (2006)	
#2	1001	Lee & Moser (2015)	
#3	1995	Lee & Moser (2015)	
#4	2003	Hoyas & Jiménez (2006)	
#5	3996	Kaneda & Yamamoto (2021)	
#6	4179	Lozano-Durán & Jiménez (2014)	
#7	5186	Lee & Moser (2015)	
#8	7987	Kaneda & Yamamoto (2021)	
#9	8016	Yamamoto & Tsuji (2018)	
#10	10049	Hoyas <i>et al.</i> (2022)	
#11	15994	priv. comm. Y. Yamamoto	

related linearly to velocity (Panton *et al.*, 2017), are not thought to be sufficiently transparent.

For all the following analyses and the construction of complete matched inner-outer asymptotic expansions, the 11 channel DNS, listed in table 1, are used.

2 A brief review of MAE and a simple test to identify overlaps in DNS profiles

In order to fix ideas and nomenclature, the essentials of MAE (see e.g. Kevorkian & Cole, 1981; Wilcox, 1995, etc.) are briefly reviewed with a presentation that is tailored to the problem at hand.

For the basic case of two scaling regions: an inner region, where the quantity of interest is described by a function $f_{in}(y)$ varying on the "fast" inner scale y , and an outer region, where it is described by $f_{out}(Y)$, which varies on the "slow" outer scale $Y = \epsilon y$. Here and in the following, f_{in} and f_{out} represent asymptotic expansions in terms of a small parameter $\mu(\epsilon)$.

To provide a description over the entire interval of interest, f_{in} and f_{out} need to be asymptotically matched across an overlap. In simple cases, such as the ones being considered here, this is achieved by requiring

$$f_{in}(y \rightarrow \infty) = f_{out}(Y \rightarrow 0) \equiv f_{OL} \quad (3)$$

In more delicate cases, however, it is necessary to introduce an intermediate variable η for the matching, with $y \gg \eta \gg Y$.

From the three f 's in (3), a composite function

$$f_{comp}(y) \equiv f_{in}(y) + f_{out}(Y) - f_{OL} \approx f_{DNS} \quad (4)$$

can be constructed to describe f_{DNS} , with the fidelity of the description depending on the number of terms carried in the expansions f_{in} and f_{out} . For the quantities analyzed in this paper, one or two terms prove sufficient to obtain asymptotic representations within the numerical uncertainty of f_{DNS} .

The decomposition

$$f_{out}(Y) = f_{OL}(Y) + W(Y) \quad , \quad (5)$$

into overlap and wake, together with relations (3-4), finally leads to

$$[f_{DNS} - f_{OL}](y) \approx [f_{in} - f_{OL}](y) + W(Y) \quad (6)$$

2.1 A test to identify overlaps

The relation (6) provides a stringent and simple means of testing whether an assumed overlap f_{OL} is indeed an overlap between inner and outer asymptotic expansions of some quantity f or not, where f_{OL} includes all higher order terms necessary for a satisfactory characterization of the overlap.

Provided f_{OL} is the correct overlap, the difference $[f_{in} - f_{OL}](y)$, by definition (3) of overlaps, goes smoothly to zero at the inner start of the overlap $y_{OL\ start}$. For $y > y_{OL\ start}$, the difference $[f_{in} - f_{OL}](y)$ remains “zero”, i.e. smaller than the uncertainties of $f_{DNS} - f_{OL}$, until $W(Y)$ becomes appreciable beyond some $Y_{W\ start}$. Hence, the only condition for this simple test to “work” is that $y_{OL\ start} < (\text{Re}_\tau Y_{W\ start})$, i.e. that Re_τ is sufficiently large.

There are two additional essential conditions to qualify f_{OL} as an overlap:

- $|f_{DNS} - f_{OL}|$ must, for all Re_τ , drop below its uncertainty level at a $y_{OL\ start}$ which is independent of Re_τ ,
- and $|f_{DNS} - f_{OL}|$ must remain below this level up to a fixed $Y_{W\ start}$.

In figure 2 both overlaps (1) and (2) for $\langle uu \rangle$ are tested. To avoid clutter, only four profiles of table 1 are shown and all clearly demonstrate that the logarithmic fit (1) does not pass the overlap test, while the overlap (2) clearly does. The same conclusion is reached with modified coefficients in (1) (not shown in fig. 2). The test (6) will be demonstrated to be also effective to identify the overlaps of $\langle ww \rangle$ and $\langle vv \rangle$ in sections 4 and 5.

When dealing with experimental profiles, the uncertainties are typically at least one order of magnitude larger than in DNS, making the identification of overlaps much more challenging. In a recent paper, Nagib & Marusic

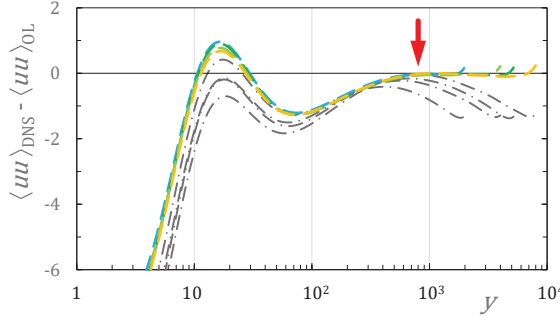


Figure 2: Difference between the profiles of $\langle uu \rangle_{\text{DNS}}$ #3, 5, 7 and 8 of table 1 and the “CS” overlap (2) (color $--$), as well as the logarithmic law (1) (grey $--\cdot--$). Vertical red arrow, start of the “CS” overlap at $y \approx 800$.

(2025) have analyzed a large number of data by dividing them by various logarithmic and power-law fitting relations. They have however not made clear which ones are proposed as overlaps. Also, the role of their starting points $y_{in} \sim \text{Re}_\tau^{1/2}$ for the ZPG and Superpipe fits is not clear, as overlaps *must* start at a fixed value of the inner coordinate y , independent of Re_τ .

For perfect data, validating an overlap by subtracting it from the data and by forming the ratio of data and presumed overlap are trivially equivalent. In practice, however, the y -dependence of the data uncertainty must be considered:

- In DNS, the step size generally increases with distance from the wall, while gradients decrease, leaving the uncertainty very roughly independent of wall distance. In this situation, subtracting the overlap from the data as in equation (6) is preferable, as the overlaps considered here are decreasing functions of y and a division would amplify the uncertainty towards the centerline.
- In experimental data, on the other hand, the uncertainty often increases dramatically towards the wall, and dividing the data by the presumed overlap may provide a more balanced view of the difference between data and overlap.

3 The stream-wise normal stress $\langle uu \rangle$

Like the MVP, the stream-wise normal stress has been extensively discussed in the literature and the question of whether $\langle uu \rangle$ is unbounded or not for $\text{Re}_\tau \rightarrow \infty$ is intimately linked to the functional form of the overlap, as discussed in the introductory section 1. As argued in section 2 and figure 2, the overlap of $\langle uu \rangle$ for the channel data in table 1 is the “CS” overlap of equation (2), shown by the red dotted lines in figure 1.

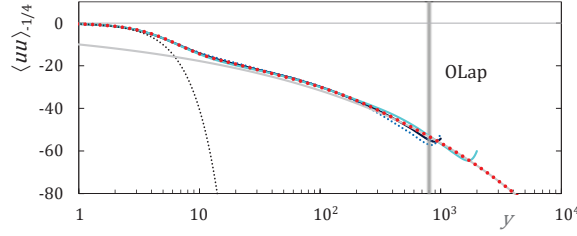


Figure 3: Order $\mathcal{O}(\text{Re}_\tau^{-1/4})$ of stream-wise normal stress $\langle uu \rangle$ extracted from DNS in fig. 1b of Monkewitz (2022) (see also Monkewitz, 2023, fig. 2). \cdots (black), 1st term $-0.405 y^2$ of Taylor series; — (grey), outer overlap $-10 y^{1/4}$; $\bullet\bullet\bullet$ (red), new complete fit (9) of the $\mathcal{O}(\text{Re}_\tau^{-1/4})$ contribution to $\langle uu \rangle$.

The complete outer expansion is obtained by adding a wake function $W(Y)$ to the overlap (2). In the following, all wakes will be modelled by the generic function $W(Y) = \Delta_1 \exp[-c_1(1-Y)] + \Delta_2 \exp[-c_2(1-Y)^2]$.

Hence, the complete outer expansion of $\langle uu \rangle$, shown in figure 1(b), is

$$\langle uu \rangle_{out}(Y) = 10.6 - 10 Y^{1/4} + W_{uu} \quad \text{with} \quad (7)$$

$$W_{uu}(Y) = 0.29 \exp[-8.621(1-Y)] - 0.07 \exp[-10(1-Y)^2], \quad (8)$$

where the product $0.29 \times 8.621 = 10/4$ ensures a zero centerline slope of $\langle uu \rangle_{out}$.

Based on the evidence of figure 2, the inner expansion, which blends into this overlap at $y \approx 800$, is of the form $\langle uu \rangle = f_0(y) + \text{Re}_\tau^{-1/4} f_1(y) + \dots$, with $f_0 \rightarrow 10.6$ and $f_1 \rightarrow -10 y^{1/4}$ for $y \gg 1$.

Here, a new complete composite expansion for $\langle uu \rangle$ is developed, which represents a significant improvement over the one in Monkewitz (2022, fig. 3), which used a “patch” at $y = 470$. In a first step, the $\mathcal{O}(\text{Re}_\tau^{-1/4})$ contribution to $\langle uu \rangle$ of Monkewitz (2022, fig. 1b) is refitted by

$$\begin{aligned} \langle uu \rangle_{in,-1/4} = & -y^{1/4} \{ 10 - 0.6 \exp(-0.00005 y^{7/4}) \\ & - 1.0 \exp(-0.006 y^{7/4}) - 8.4 \exp(-0.047 y^{7/4}) \} \end{aligned} \quad (9)$$

and shown in figure 3. The above coefficients yield the best fit Taylor expansion $\langle uu \rangle_{in,-1/4} = -0.405 y^2 + \dots$.

Subtracting the order $\mathcal{O}(\text{Re}_\tau^{-1/4})$ of equation (9) from the DNS yields the leading order of the inner expansion $\langle uu \rangle_{in,0}$, shown in figure 4. The large

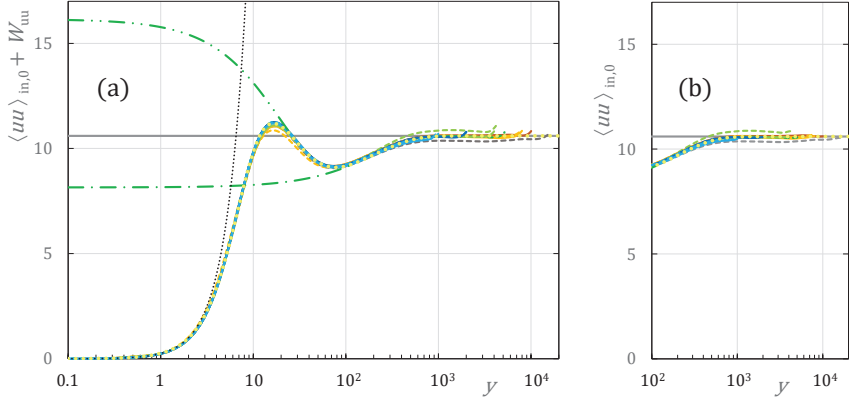


Figure 4: Order $\mathcal{O}(1)$ of stream-wise normal stress $\langle uu \rangle_{in,0}$ (10-12) plus wake (8) in panel (a) and without wake in (b). \cdots (black), 1st term $(1/4)y^2$ of Taylor series; — (grey), small- Y limit 10.6 of overlap; $-\cdot-\cdot-$ (green), exponential (10); $-\cdot-\cdot-$ (green), exponential (11); $\bullet\bullet\bullet$ (light yellow), complete inner fit (10-12) of the $\mathcal{O}(1)$ contribution to $\langle uu \rangle$.

majority of data are seen to collapse very nicely onto the sum of exponentials

$$\langle uu \rangle_{in,0} = 10.6 - 2.45 \exp(-0.005 y) \quad (10)$$

$$+ 8 \exp(-0.05 y) \quad (11)$$

$$- 16.15 \exp(-0.02401 y - 0.01639 y^2 - 1.0317 10^{-5} y^3 \\ + 4.1 10^{-5} y^4 - 1.1 10^{-6} y^5) , \quad (12)$$

where the coefficients of y to y^4 in the last exponential (12) are determined such as to produce the best fit Taylor expansion $(1/4)y^2$ about the wall for $\langle uu \rangle_{in,0}$.

The description of the damped oscillations of $\langle uu \rangle_{in,0}$ in terms of simple exponentials finally provides a straightforward characterization of their spatial scales by the coefficients in the exponents: The first two exponentials (10-11) yield scales of $(0.005)^{-1} = 200$ and $(0.05)^{-1} = 20$. Since the last exponential (12) has a complicated argument, constrained to produce the best fit Taylor expansion, the shortest scale is taken to be the intersection of the Taylor expansion with the asymptotic value 10.6 of $\langle uu \rangle_{in,0}$ (equ. 10), i.e. $(4 \times 10.6)^{1/2} \approx 6.5$, which is of the order of the viscous sublayer thickness. This sequence of length scales will be compared in the final section 7 to the sequence of scales characterizing the spatial oscillations of the MVP indicator function educed in section 6.

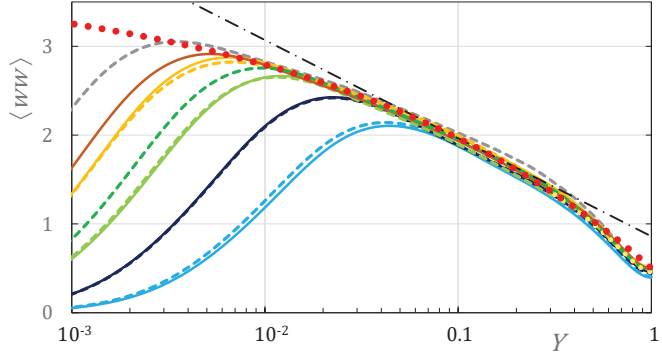


Figure 5: Cross-stream normal stress $\langle ww \rangle$ versus Y . $\bullet\bullet\bullet$ (red), overlap (13); $\bullet\bullet\bullet$ (light yellow), full outer expansion (15); $-\cdot-\cdot-$ (black), logarithmic fit $0.86 - 0.48 \ln Y$.

4 The cross-stream normal stress $\langle ww \rangle$

The cross-stream stress $\langle ww \rangle$ is shown in figure 5 for the DNS of table 1. As for the stream-wise stress, the “bounded dissipation” overlap

$$\langle ww \rangle_{OL} = 3.85 - 3.40 Y^{1/4} , \quad (13)$$

is seen in figure 5 to closely fit the data from $y \approx 60$ all the way to $Y \approx 0.4$, while the example of a logarithmic fit hugs the data only over the short interval $Y \in [0.1, 0.2]$. An alternative logarithmic tangent at smaller Y , say 0.01, not shown in figure 5, would in turn correspond to an overlap with an outer end at the suspiciously small value of $Y \approx 0.02$.

The test of overlap (13) devised in section 2 is shown in figure 6(a). While the “CS” overlap (13) does not look quite as convincing as the one for $\langle uu \rangle$ in figure 2, it appears clearly superior to the example of a logarithmic law. A straightforward extension of the overlap fit (13) to

$$\langle ww \rangle_{OL+} = 3.87 - 3.40 Y^{1/4} + 0.3 Y - 200 \text{Re}_\tau^{-1} \quad (14)$$

actually resolves the problem almost perfectly in figure 6(b), in which the #10 profile of table 1 has been added to show how the narrow computational box of this DNS affects the $\langle ww \rangle$ overlap. Figure 6(b) also shows a slight “hump” at $y \approx 75$, ahead of the overlap starting at $y \approx 150$.

This refined overlap analysis demonstrates that equation (13) is a valid low-order approximation of the overlap. However, to avoid developing a matching correction of order $\mathcal{O}(\text{Re}_\tau^{-1})$ for the inner expansion, which is not essential to the understanding of the asymptotic structure of $\langle ww \rangle$, the basic overlap (13) is used in the following. With this, the question of overlap is resolved in favor of the “CS” version (13), leading to the outer expansion of

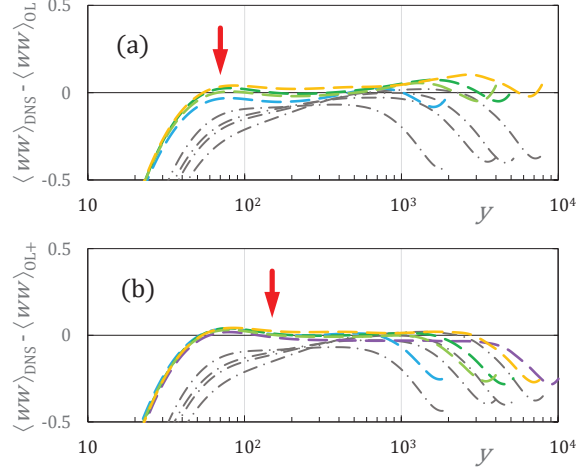


Figure 6: (a) Difference between the profiles of $\langle ww \rangle_{DNS}$ #3, 5, 7 and 8 of table 1 and the “CS” overlap (13) (color $--$), as well as the logarithmic law $0.86 - 0.48 \ln Y$ (grey $--\cdots-$). Vertical red arrow, start of the “bounded dissipation” overlap at $y \approx 70$. (b) Same data as in (a) plus profile #10, minus the expanded overlap (14). Vertical red arrow, start of the overlap moved to $y \approx 150$

$$\langle ww \rangle$$

$$\langle ww \rangle_{out}(Y) = 3.85 - 3.40 Y^{1/4} + W_{ww}(Y) \quad \text{with} \quad (15)$$

$$W_{ww}(Y) = 0.14 \exp[-6.071(1-Y)] - 0.18 \exp[-6(1-Y)^2], \quad (16)$$

where the product $0.14 \times 6.071 = 3.40/4$ ensures a zero centerline slope of $\langle ww \rangle_{out}$.

As for $\langle uu \rangle$, the inner expansion of $\langle ww \rangle$ must be of the form $\langle ww \rangle = f_0(y) + \text{Re}_\tau^{-1/4} f_1(y) + \dots$, with $f_0 \rightarrow 3.85$ and $f_1 \rightarrow -3.40 y^{1/4}$ for $y \gg 1$ in order to asymptote to the overlap (13). This is achieved by the simple fit for the $\text{Re}_\tau^{-1/4}$ term in the inner expansion

$$\langle ww \rangle_{in, -1/4} = -3.40 y^{1/4} \{1 - \exp(-0.047 y^{7/4})\} \quad (17)$$

Subtracting the higher order term (17) from the DNS yields the infinite Reynolds number limit $\langle ww \rangle_{in, 0}$ of the inner expansion in figure 7.

As $\langle ww \rangle_{in, 0}$ shows no oscillations, the Padé approximant (18), indicated by the yellow dots in figure 7, is well adapted to fit $\langle ww \rangle_{in, 0}$:

$$\langle ww \rangle_{in, 0} = \{ 0.09 y^2 + 0.0018 y^4 + 2 \cdot 10^{-10} y^8 \} \times \{ 1 + 0.067 y^2 + 0.000465 y^4 + (2 \cdot 10^{-10}/3.85) y^8 \}^{-1} \quad (18)$$

With the complete outer expansion (15, 16), the full composite expansion of $\langle ww \rangle$ is finally

$$\langle ww \rangle_{comp} = \langle ww \rangle_{in, 0} + \text{Re}_\tau^{-1/4} \langle ww \rangle_{in, -1/4} + W_{ww}(Y) , \quad (19)$$

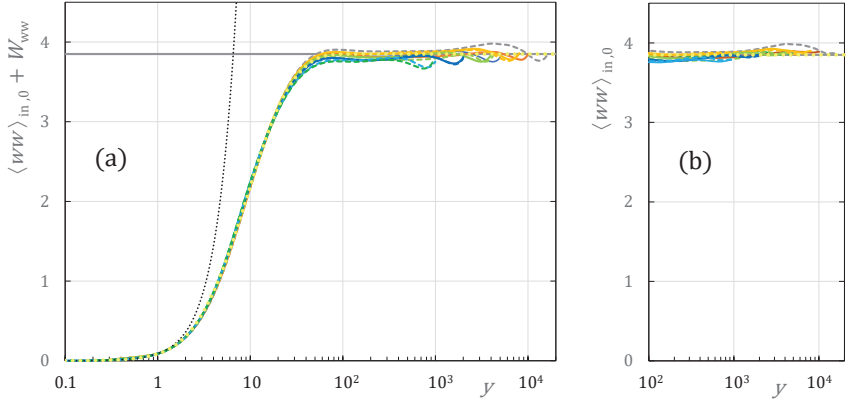


Figure 7: Order $\mathcal{O}(1)$ of cross-stream normal stress $\langle ww \rangle_{in,0}$ (18) plus wake (8) in panel (a) and without wake in (b). \cdots (black), 1st term $0.09 y^2$ of Taylor series; — (grey), small- Y limit 3.85 of outer overlap; $\bullet\bullet\bullet$ (light yellow), complete inner fit (18) of the $\mathcal{O}(1)$ contribution to $\langle uu \rangle$.

where $W_{ww}(Y)$ is given by equation (16).

5 The wall-normal stress $\langle vv \rangle$

Compared to the stream-wise Reynolds stress, the wall-normal stress has received less attention, except for the case of rough walls, where $\langle vv \rangle$ plays a key role in the interactions between ground and atmosphere (see for instance Orlando, 2013). There exist also very few data fits to corroborate proposed scalings - one specific proposal is the Taylor series of $\langle vv \rangle$, fitted by an expansion in $\ln \text{Re}_\tau$ by Smits *et al.* (2021), which is however not supported by the following complete analysis.

To develop the first full MAE description of $\langle vv \rangle$, it is useful to first inspect the set of data in table 1, plotted against both outer and inner wall-normal coordinates in figures 8(a) and (b) (note that profile #11 differs significantly from all the others and will in the following be disregarded for the fits). Several features of $\langle vv \rangle$ in this figure are noteworthy: After the rise close to the wall, corresponding to the inner expansion, the decaying parts in figure 8(a) are progressively shifted down as Re_τ is decreased, by amounts that are to a good approximation independent of Y . The second significant feature of figure 8(a) is the gradual departure of $\langle vv \rangle$ from the linear fit $(1.39 - 1.14 Y)$ below $Y \approx 0.15$.

This departure is reproduced by the overlap

$$\langle vv \rangle_{OL} = 1.31 - 1.18 Y^{5/4} - 500 \text{Re}_\tau^{-5/4} , \quad (20)$$

which is seen in figure 8(b) to nearly perfectly reproduce the Re_τ -dependent

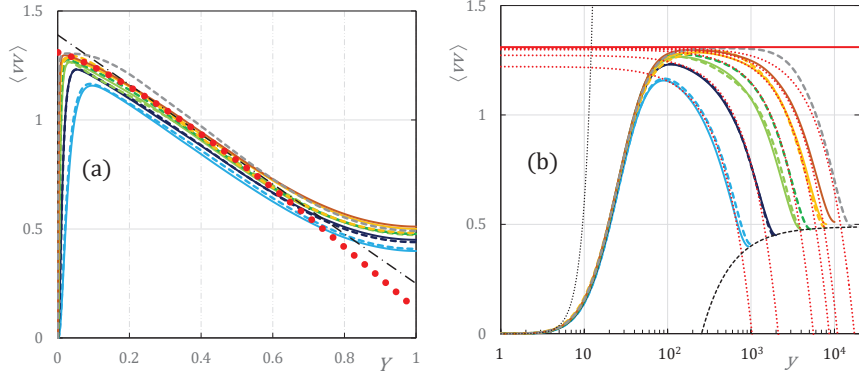


Figure 8: (a) Wall-normal stress $\langle vv \rangle$ versus Y . $\bullet\bullet\bullet$ (red), overlap (20) for infinite Re_τ ; $-\cdot-\cdot-$ (black), linear fit $1.39 - 1.14 Y$ to guide the eye. (b) $\langle vv \rangle$ versus y . \cdots (black), 1st term $0.00015 y^4$ of Taylor series; $---$ (black), equ. (21) for the centerline $\langle vv \rangle_{CL}$; — (red), overlap (20) at $Re_\tau = \infty$; \cdots (red), overlaps at selected finite Re_τ .

shifts and the negative curvature of $\langle vv \rangle$ towards the wall (again, disregarding profile #11).

The choice of the $Re_\tau^{-5/4}$ scaling is again verified by the test devised in section 2, shown in figure 9, where (20) is compared to the linear fit $1.39 - 1.14 Y$. Further support for the overlap (20) comes from the excellent fit of the centerline $\langle vv \rangle_{CL}$ seen in figure 8(b)

$$\langle vv \rangle_{CL} = 0.49 - 500 Re_\tau^{-5/4} \quad , \quad (21)$$

where $y = Re_\tau$. Note that the difference between $1.31 - 1.18 = 0.13$ in equation (20) and 0.49 in equation (21) is the value of the wake function

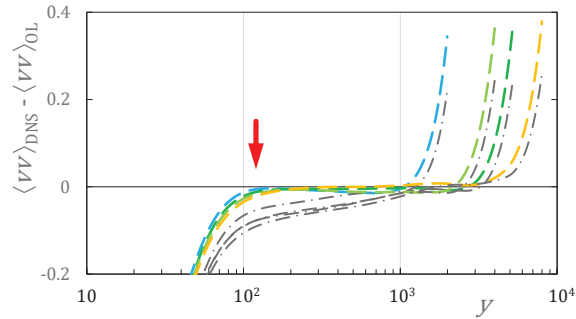


Figure 9: Difference between the profiles of $\langle vv \rangle_{DNS}$ #3, 5, 7 and 8 of table 1 and the overlap (20) (color $--$), as well as the linear fit $1.39 - 1.14 Y$ (grey $-\cdot-\cdot-$). Vertical red arrow, start of the overlap at $y \approx 120$.

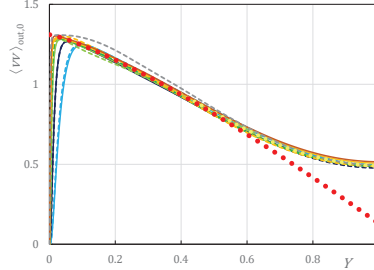


Figure 10: Infinite Re_τ limit of outer wall-normal stress $\langle vv \rangle_{out}$ (equ. 23) versus Y . $\bullet\bullet\bullet$ (red), overlap (20) at infinite Re_τ ; $\bullet\bullet\bullet$ (light yellow), infinite Re_τ limit of full outer expansion (24).

(22) on the centerline. The latter is well fitted by

$$W_{vv}(Y) = 0.36 \exp [-4.0972 (1 - Y) - 8 (1 - Y)^{5/2}] \quad , \quad (22)$$

where the coefficient of $(1 - Y)$ is adjusted to yield a zero centerline slope for the outer expansion $\langle vv \rangle_{out}$, given by

$$\langle vv \rangle_{out} = \langle vv \rangle_{out,0} + \text{Re}_\tau^{-5/4} \langle vv \rangle_{out,-5/4} \quad \text{with} \quad (23)$$

$$\langle vv \rangle_{out,0} = 1.31 - 1.18 Y^{5/4} + W_{\langle vv \rangle}(Y) \quad (24)$$

$$\langle vv \rangle_{out,-5/4} = -500 \quad (25)$$

Figure 10 shows the infinite Re_τ limit $\langle vv \rangle_{out,0} = \langle vv \rangle_{DNS} - \text{Re}_\tau^{-5/4} \langle vv \rangle_{out,-5/4}$, together with the infinite Re_τ limits of the overlap 20 and of the full fit of $\langle vv \rangle_{out,0}$ given by equation (24).

Turning to the inner expansion of order $\mathcal{O}(\text{Re}_\tau^{-5/4})$, the uniform outer offset (25) of order $\mathcal{O}(\text{Re}_\tau^{-5/4})$ has to be brought smoothly down to zero at the wall. This is achieved with a simple Padé approximant which produces the appropriate Taylor series of $\langle vv \rangle$ about the wall, starting with y^4 . Hence, the full $\mathcal{O}(\text{Re}_\tau^{-5/4})$ contribution $\langle vv \rangle_{in,-5/4}$ matching the overlap (20) for $y \gg 1$ is

$$\langle vv \rangle_{in,-5/4} = -500 \frac{2 \cdot 10^{-7} y^4}{1 + 2 \cdot 10^{-7} y^4} - 1.18 y^{5/4} \quad (26)$$

Subtracting $\text{Re}_\tau^{-5/4}$ times equation (26) from the DNS leads in figure 11 to a good overall data collapse for $\langle vv \rangle_{in,0}$ (again with the exception of profile #11), which becomes excellent below $y \approx 50$. To develop a consistent model for $\langle vv \rangle_{in,0}$, its approach to the constant 1.31 at large y needs to be determined. This amounts to finding how the location of the maximum of $\langle vv \rangle$ scales with Re_τ . The Reynolds number scaling of the $\langle vv \rangle$ maxima is shown in figure 12. Up to Re_τ of 5200, their location is well described by

$$Y_{max\ vv} = 16.5 \text{Re}_\tau^{-3/4} \quad (27)$$

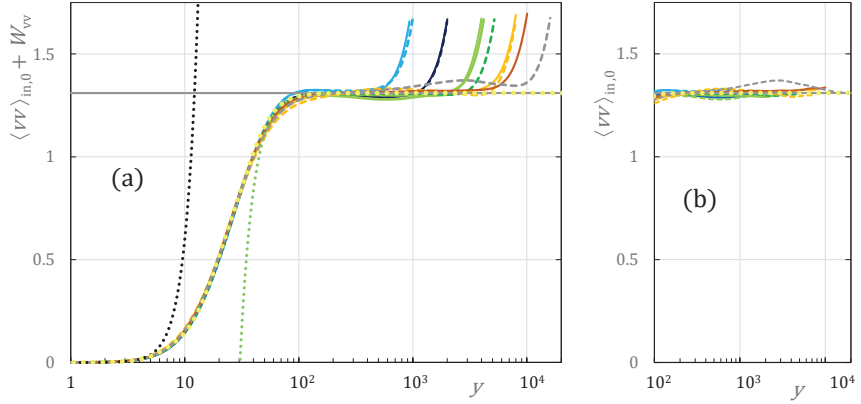


Figure 11: Infinite Re_τ limit of inner wall-normal stress $\langle vv \rangle_{DNS} - Re_\tau^{-5/4} \langle vv \rangle_{in,-5/4}$ plus the wake (22) versus y in (a) and without the wake in (b). $\bullet\bullet\bullet$ (red), fit (30); \cdots (black), Taylor expansion $6 \cdot 10^{-5} y^4$; \cdots (aqua), asymptotic approach to 1.31, equal to the 1st two terms of equ. (28), with $C = 4.81 \cdot 10^5$ and $\alpha = 15/4$.

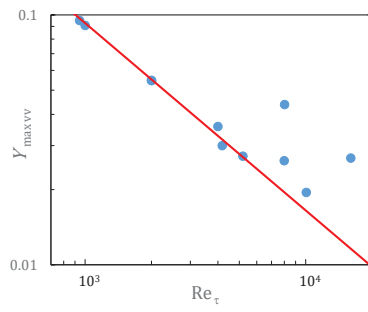


Figure 12: Location of the maxima (blue \bullet) of $\langle vv \rangle$ for the DNS of table 1. — (red), $16.4 Re_\tau^{-3/4}$.

and the scatter beyond is attributed to increasing uncertainties of the DNS.

The “local composite expansion” of $\langle vv \rangle$ in a neighborhood of its maximum around $y \approx 10^2$ is of the form

$$\langle vv \rangle \cong 1.31 - C y^{-\alpha} - 500 \text{Re}_\tau^{-5/4} - 1.18 Y^{5/4} , \quad (28)$$

where C and α are to be determined. The maximum of (28) is obtained from its derivative

$$Y_{max\,vv}^{(5/4+\alpha)} = \left\{ \frac{4\alpha C}{5 \times 1.18} \right\} \text{Re}_\tau^{-\alpha} . \quad (29)$$

Combining equations (27) and (29) yields $\alpha = 15/4$ and $C = 4.81 \cdot 10^5$, and leads to the Padé approximant

$$\begin{aligned} \langle vv \rangle_{in,0} = & \{6.2 \cdot 10^{-5} y^4 + 2.5 \cdot 10^{-7} y^6 + 6.6 \cdot 10^{-9} y^8 + 1.2 \cdot 10^{-14} y^{47/4}\} \\ & \times \{1 + 7.7 \cdot 10^{-4} y^4 + 1. \cdot 10^{-6} y^6 + +8.4 \cdot 10^{-9} y^8 + (1.2/1.31) \cdot 10^{-14} y^{47/4}\}^{-1} \end{aligned} \quad (30)$$

which has both the appropriate Taylor expansion and the best fit asymptotic expansion. This completes the full MAE description of $\langle vv \rangle$, summarized by the composite expansion

$$\langle vv \rangle_{comp} = \langle vv \rangle_{in,0} + \text{Re}_\tau^{-5/4} \langle vv \rangle_{in,-5/4} + W_{vv}(Y) \quad (31)$$

given by equations (30), (26) and (22).

6 The log indicator function for the mean velocity

Although there exists an extensive literature on turbulent MVPs, this author is not aware of a high fidelity full, meaning from wall to centerline, matched asymptotic description of the channel MVP, which captures its subtle slope variations. To clearly reveal the latter, the logarithmic indicator function

$$\Xi = y dU/dy = Y dU/dY \quad (32)$$

is examined here. To describe the inner part, a sum of exponentials again proves useful, as each simple exponential explicitly reveals the scale of the associated slope change:

$$\Xi_{in}(y) = \frac{1}{0.417} + 0.27 \exp(-0.0007 y) \quad (33)$$

$$- 0.7 \exp(-0.009 y) \quad (34)$$

$$+ 9 \exp(-0.073 y) \quad (35)$$

$$\begin{aligned} - 10.97 \exp(-0.1505 y - 9.144 \cdot 10^{-3} y^2 - 8.612 \cdot 10^{-4} y^3) \\ + 1.18 \cdot 10^{-4} y^4 - 5. \cdot 10^{-6} y^5 \end{aligned} \quad (36)$$

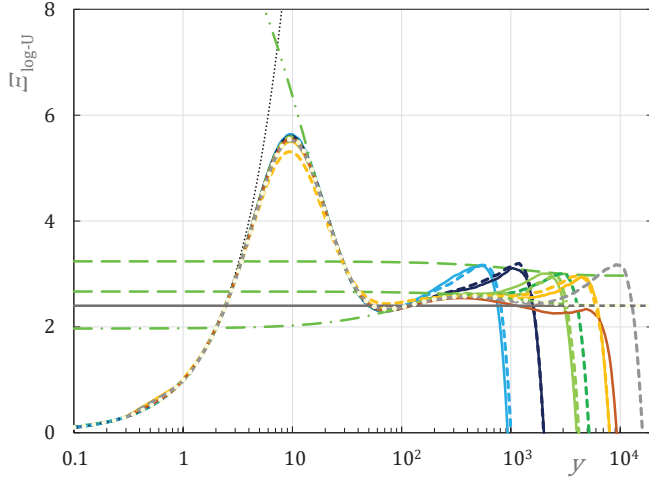


Figure 13: Logarithmic indicator functions $y (dU/dy)$ of the mean velocity for the CFD's of table 1. Color and line styles as in the table. — (grey), $\Xi = 2.4$ ($\kappa = 0.417$); - - - (green), exponential (33) plus its up-shifted image; - - - - (green), exponential (34); - - - - - (green), exponential (35); (black), 1-term Taylor expansion (37); ••• (light yellow), full inner fit (33-36).

The coefficients of y to y^4 in the last exponential (36) are determined such as to produce the Taylor expansion

$$\Xi_{in} = y - 1.295 10^{-3} y^4 + H.O.T. \quad (37)$$

about the wall, deduced in Monkewitz (2024, equ. 7).

The fit (33-36) of the inner $\Xi_{in}(y)$ is shown as yellow dots in figure 13 and is seen to provide an exceptionally good model for all but two DNS, up to the point where Ξ develops outer-scaled “humps” above the overlap ($1/0.417$) (the grey horizontal line in figure 13). No finite Re_τ corrections to the above $\Xi_{in}(y)$ are considered here. If there are any, they are of the order of the data uncertainty and cannot be determined reliably.

The outer expansion is modeled as

$$\Xi_{out}(Y) = \frac{1}{0.417} \quad (38)$$

$$+ 0.05 \ln\{1 + \exp[32(Y - 0.13)]\} \quad (39)$$

$$- C \ln\{1 + \exp[2000(Y - 0.36)^3]\} \quad \text{with}$$

$$C = 1.907 10^{-3} [\Xi_{in}(y = Re_\tau) + 1.392] \quad (40)$$

where the first term (38) is the common part or overlap ($1/0.417$) of inner and outer expansions and the terms (39) plus (40) are the wake function. Its first part (39) represents a quasi-linear departure from the inner expansion,

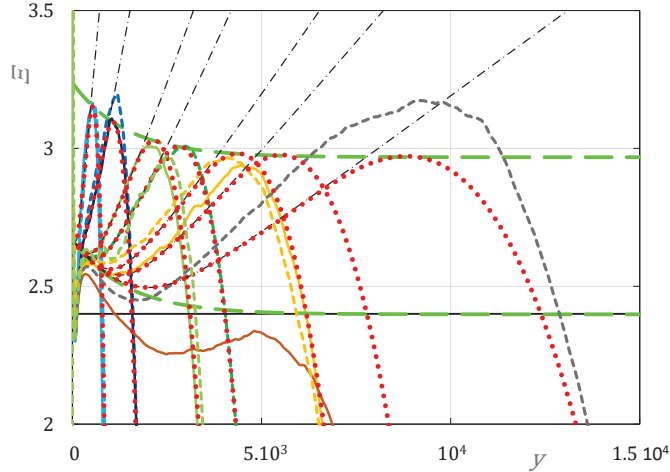


Figure 14: Same as figure 13 on linear scale. — (grey), $\Xi = 2.4$ ($\kappa = 0.417$); - - - (green), exponential (33) plus its up-shifted image; • • • (red), outer quasi-linear parts and decays to the CL; - - - (thin black), outer quasi-linear parts (39) only.

branching off Ξ_{in} at $Y = 0.13$, and the coefficient C of last term (40) is adjusted such that the additive composite expansion

$$\Xi_{comp} = \Xi_{in}(y) + \Xi_{out}(Y) - \frac{1}{0.417}, \quad (41)$$

is zero on the centerline.

This composite expansion (41) is shown in figure 14 and calls for two comments:

- The first concerns the quasi-linear part of equation (39), shown in figure 14 as thin black $-\cdot-\cdot-$ lines for the different Re_τ . These lines peel off the inner expansion at the fixed outer Y of 0.13 and have no matching inner part. This is because the quasi-linear part in question has been designed to go to zero exponentially for $Y \ll 0.13$ (see e.g. Wilcox, 1995, for a discussion of transcendentally small terms in MAE). Note that the absence of a matching higher order linear term $\propto y/Re_\tau$ in the inner expansion, proposed in Monkewitz & Nagib (2023), is consistent with the latest conclusions of Nagib & Marusic (2025).

As shown in the above papers and references therein, the slope of the quasi-linear region (39) is strongly flow-dependent. This will be further discussed in the concluding section 7.

- The second comment concerns the progressively important deviations of the data from the outer fits as Re_τ increases. Up to profile #7 of

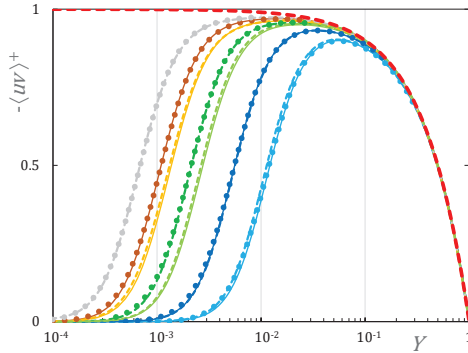


Figure 15: Negative Reynolds stress $-\langle uv \rangle$ for the DNS of table 1. - - - (red), asymptote $(1 - Y)$. ● ● ●, composite fits of $-\langle uv \rangle$ for the Re_τ 's of DNS #1,4,7,10 and 11, obtained from the fit (41) of Ξ_{comp} and the mean momentum equation.

table 1, the DNS for similar Re_τ 's are reasonably well fitted by the composite expansion (41). Beyond Re_τ 's of around 5000, however, the computed Ξ become progressively more erratic and the difference between equation (41) and the DNS quickly grows beyond 10% in the region $y > 10^2$, indicating that the limits of current DNS have been reached for Ξ . This is consistent with the demonstration in Monkewitz (2024, fig. 4), that the Ξ determined from the computed Reynolds stress $\langle uv \rangle$ and the mean momentum equation differ significantly from figure 14.

This naturally raises the question of justification for the fit of Ξ_{out} by equations (38-40) at large Re_τ . A first support comes from inverting the argument of Monkewitz (2024) and compute the Reynolds stress from the composite expansion 41 of Ξ and the mean momentum equation. This is shown in figure 15 and supports the present composite expansion 41 “within drawing accuracy” up to the highest Re_τ available.

To further validate the composite fit (41), it is divided by y and integrated from wall to centerline in order to obtain the fitted centerline velocity U_{CL} , which is shown in figure 16 to be in excellent agreement with the DNS considered here, except again with DNS #10.

From the above discussion of the channel MVP and from figure 13 in particular, it is evident that, at the Re_τ 's available today, it is hazardous to estimate the Kármán parameter κ from the indicator function Ξ . This conclusion is of course not new, as it has been reached long ago by Coles (1956), who always advocated using the Re_τ dependence of centerline or free-stream velocity to determine κ . What is new here, is the determination of the complete Ξ with its oscillations and false “flats” that can be and have

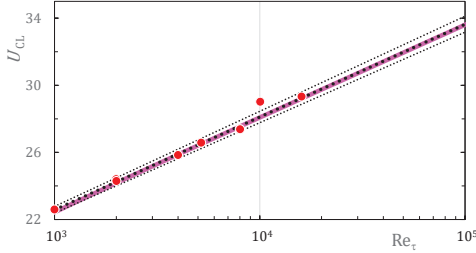


Figure 16: Centerline velocities for the cases of table 1; \bullet (red) DNS; — (pink), CL velocities from integrating the full fit for Ξ/y^+ . \cdots (black), $6 + 2.4 \ln \text{Re}_\tau$ with slopes modified by $\pm 2.5\%$.

been mistaken for logarithmic overlaps.

The present analysis also illustrates the power of asymptotic analysis to extract the correct overlap from data at relatively low Re_τ , at which the overlap $\Xi_{OL} = 2.4$ is contaminated from both sides by inner and outer terms. To actually start seeing the clean overlap, the inner expansion (33-36) would have to closely approach the overlap (1/0.417), *before* the outer expansion (39-40) starts to significantly deviate from it. This is the case when both $y \gtrsim 4000$ (see fig. 13) and $Y \lesssim 0.08$ (see fig. 14). Such a scale separation is only attained for $\text{Re}_\tau > 5 \cdot 10^4$, clearly beyond the reach of DNS in the foreseeable future.

Finally, the spatial oscillations of Ξ_{in} in figure 13 are characterized like those of $\langle uu \rangle_{in,0}$ at the end of section 3. The first three simple exponentials in equations (33-35) yield length scales of $(0.0007)^{-1} \approx 1400$; $(0.009)^{-1} \approx 110$ and $(0.073)^{-1} \approx 14$. The smallest scale of 2.4 is again obtained from the intersection of the leading term y in the Taylor expansion (37) with the asymptotic value of $\Xi_{in} = 1/0.417$, and is of the order of the viscous sublayer thickness. These observations are compared to the oscillations of $\langle uu \rangle_{in,0}$ in the following concluding section 7.

7 Closing comments

The asymptotic expansions in sections 3-6 provide optimal descriptions of all first and second order moments in turbulent channel flow obtained from current DNS, as the Reynolds stress $\langle uv \rangle$ is easily obtained from Ξ and the mean momentum equation, as shown in figure 15. The inverse, however, i.e. obtaining Ξ from $\langle uv \rangle$ and the momentum equation, is not possible with the currently available DNS, as shown by Monkewitz (2024, fig. 4), and one to two additional significant digits would be required beyond $y \approx 50$ to remedy the situation.

Next, a comment is necessary on the asymptotic sequence used throughout this study, which progresses in $1/4$ powers of Re_τ , while several authors

(for instance Pirozzoli, 2024) have advocated various correlations with “odd” powers of Re_τ . The important difference is that these “odd” powers have been proposed to fit *total* quantities, while in the present study the $n/4$ powers of Re_τ represent the scaling of *individual terms in asymptotic expansions*. At any rate, it is difficult to imagine how complex conservation laws, such as Reynolds stress transport equations, could be balanced order by order with “odd” powers of Re_τ already in the expansions of the most basic turbulence quantities, but the question remains open.

Regarding the rather surprising scaling of $\langle vv \rangle$, it would be interesting to test it independently. Such a test can be devised by taking the incompressible continuity equation in terms of outer-scaled coordinates, multiplying by v and time averaging, resulting in

$$\langle v \frac{\partial u}{\partial X} \rangle + \langle v \frac{\partial v}{\partial Y} \rangle + \langle v \frac{\partial w}{\partial Z} \rangle = 0 \quad (42)$$

From this, one obtains in the region of the $\langle vv \rangle$ overlap (20) a prediction for the correlation $\langle v (\partial u / \partial X) \rangle$ without adjustable parameters

$$\frac{1}{2} \frac{d\langle vv \rangle}{dY} = - \langle v \frac{\partial u}{\partial X} \rangle = - \frac{5}{8} 1.18 Y^{1/4} \quad (43)$$

The present first complete inner-outer matched asymptotic expansions should be a good starting point to develop refined models for the near-wall turbulence structures. Of particular interest would be a structural model which reproduces the subtle oscillations of dU/dy , amplified in figure 13 by the multiplication with y , and those of $\langle uu \rangle$, which may or may not be connected. The spatial scales of these oscillations, obtained from the sequence of exponentials in the fit (33-35) for Ξ_{in} and from the fit (10-11) for $\langle uu \rangle_{in,0}$, are shown in figure 17, together with the speculative correlation

$$scale = 0.4 e^{2n} \quad (44)$$

A connection may exist between these oscillations and the various layers discussed in Wei *et al.* (2005), Klewicki *et al.* (2007) and Klewicki (2013b,a), but more diagnostics will be required to arrive at a structure based explanation.

Finally, coming back to the MVP, it is recalled that the slope of the “quasi-linear” part in equation (39) for the outer indicator function Ξ_{out} (see fig. 14) is specific to the channel. In pipes this slope is about twice the channel slope, which led Luchini (2017) to the conclusion that it is proportional to the mean pressure gradient. The extensive data analysis of Monkewitz & Nagib (2023) did however not support this exact proportionality, but the physical origin of the quasi-linear region (39) remains to be elucidated.

The comparison of channel, pipe and ZPG boundary layer MVPs in the final figure 18 reveals that the ZPG TBL exhibits by far the largest slope

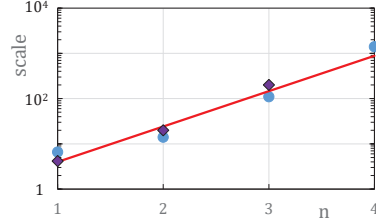


Figure 17: Consecutive wall-normal scales associated with the oscillations of Ξ and $\langle uu \rangle$ in figures 13 and 4: • (blue), sequence of oscillation scales for the MVP indicator function Ξ (equ. 33-36); ♦ (violet), analogue for $\langle uu \rangle$ (equ. 10-12). — (red), speculative fit (44).

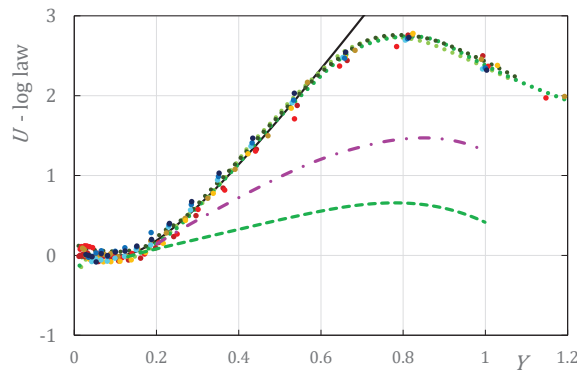


Figure 18: Mean velocity profiles minus log-laws $(1/\kappa) \ln \text{Re}_\tau + B$. ••• (different colors), ZPG TBLs from fig. 7 of Monkewitz & Nagib (2023) ($\kappa = 0.384, B = 4.17$); - - - (green), channel DNS #7 ($\kappa = 0.417, B = 5.65$); - · - - (violet), pipe DNS of Pirozzoli *et al.* (2021) at $\text{Re}_\tau = 6000$ ($\kappa = 0.433, B = 6.65$).

of the quasi-linear region of all three MVPs. Hence, a connection between quasi-linear slope and the mean pressure gradient appears tenuous, and a new “geometric” explanation is proposed here. Relative to the channel, the span-wise space in the pipe is reduced towards the centerline by a factor $(1 - Y)$, which is thought to “squeeze” the outer turbulence structures in the z direction, thereby enhancing $\langle uv \rangle$ and dU/dy . In the ZPG TBL, the even stronger enhancement is thought to be caused by the intrusion of high momentum free-stream fluid into the boundary layer (see for instance Chauhan *et al.*, 2014). This basic explanation could possibly be tested in pipes with solid or free slip central cores of varying diameter.

The author is grateful to Yoshinobu Yamamoto for sharing his unpublished Channel DNS.

References

CHAUHAN, K., PHILIP, J., DESILVA, CH. M., HUTCHINS, N. & MARUSIC, I. 2014 The turbulent/non-turbulent interface and entrainment in a boundary layer. *J. Fluid Mech.* **742**, 119–151.

CHEN, XI & SREENIVASAN, KATEPALLI R. 2021 Reynolds number scaling of the peak turbulence intensity in wall flows. *Journal of Fluid Mechanics* **908**, R3.

CHEN, XI & SREENIVASAN, KATEPALLI R. 2022 Law of bounded dissipation and its consequences in turbulent wall flows. *Journal of Fluid Mechanics* **933**, A20.

CHEN, XI & SREENIVASAN, KATEPALLI R. 2023 Reynolds number asymptotics of wall-turbulence fluctuations. *Journal of Fluid Mechanics* **976**, A21.

CHEN, XI & SREENIVASAN, KATEPALLI R. 2025 Bounded dissipation law and profiles of turbulent velocity moments in wall flows. *PNAS* **122** (17), e2502265122.

COLES, D. E. 1956 The law of the wake in the turbulent boundary layer. *J. Fluid Mech.* **1**, 191–226.

HOYAS, S. & JIMÉNEZ, J. 2006 Scaling of the velocity fluctuations in turbulent channels up to $Re_\tau = 2003$. *Phys. Fluids* **18**, 011702.

HOYAS, SERGIO, OBERLACK, MARTIN, ALCÁNTARA-ÁVILA, FRANCISCO, KRAHEBERGER, STEFANIE V. & LAUX, JONATHAN 2022 Wall turbulence at high friction reynolds numbers. *Phys. Rev. Fluids* **7**, 014602.

KANEDA, YUKIO & YAMAMOTO, YOSHINOBU 2021 Velocity gradient statistics in turbulent shear flow: an extension of kolmogorov's local equilibrium theory. *Journal of Fluid Mechanics* **929**, A13.

KEVORKIAN, J. & COLE, J. D. 1981 *Perturbation methods in applied mathematics*. Springer.

KLEWICKI, J. C. 2013a A description of turbulent wall-flow vorticity consistent with mean dynamics. *Journal of Fluid Mechanics* **737**, 176–204.

KLEWICKI, J. C. 2013b Self-similar mean dynamics in turbulent wall flows. *Journal of Fluid Mechanics* **718**, 596–621.

KLEWICKI, J. C., FIFE, P., WEI, T. & McMURTRY, P. 2007 A physical model of the turbulent boundary layer consonant with mean momentum balance structure. *Phil. Trans. R. Soc. Lond. A* **365**, 823–839.

LEE, M. & MOSER, R. D. 2015 Direct numerical simulation of turbulent channel flow up to $Re_\tau = 5200$. *J. Fluid Mech.* **774**, 395–415.

LOZANO-DURÁN, A. & JIMÉNEZ, J. 2014 Effect of the computational domain on direct numerical simulations of turbulent channels up to $Re_\tau = 4200$. *Phys. Fluids* **26**, 011702.

LUCHINI, PAOLO 2017 Universality of the turbulent velocity profile. *Phys. Rev. Lett.* **118**, 224501.

MARUSIC, IVAN & MONTY, JASON P. 2019 Attached eddy model of wall turbulence. *Annual Review of Fluid Mechanics* **51** (1), 49–74, arXiv: <https://doi.org/10.1146/annurev-fluid-010518-040427>.

MARUSIC, I., MONTY, J. P., HULTMARK, M. & SMITS, A. J. 2013 On the logarithmic region in wall turbulence. *J. Fluid Mech. Rapids* **716**, R3–1–R3–11.

MONKEWITZ, PETER A. 2022 Asymptotics of streamwise Reynolds stress in wall turbulence. *Journal of Fluid Mechanics* **931**, A18.

MONKEWITZ, PETER A. 2023 Reynolds number scaling and inner-outer overlap of stream-wise Reynolds stress in wall turbulence. *arXiv* **2307.00612**.

MONKEWITZ, PETER A. 2024 On the difficulty of determining Kármán “constants” from direct numerical simulations. *Physics of Fluids* **36** (4), 045162.

MONKEWITZ, PETER A. & NAGIB, HASSAN M. 2023 The hunt for the Kármán ‘constant’ revisited. *Journal of Fluid Mechanics* **967**, A15.

NAGIB, HASSAN & MARUSIC, IVAN 2025 A method for evaluating relations of turbulent normal stresses by experimental data over a wide range of reynolds numbers. *Journal of Fluid Mechanics* **1016**, A24.

ORLANDI, P. 2013 The importance of wall-normal reynolds stress in turbulent rough channel flows. *Physics of Fluids* **25** (11), 110813, arXiv: https://pubs.aip.org/aip/pof/article-pdf/doi/10.1063/1.4819348/13379985/110813_1_online.pdf.

PANTON, RONALD L., LEE, MYOUNGKYU & MOSER, ROBERT D. 2017 Correlation of pressure fluctuations in turbulent wall layers. *Phys. Rev. Fluids* **2**, 094604.

PERRY, A. E., HENBEST, S. M. & CHONG, M. S. 1986 A theoretical and experimental study of wall turbulence. *J. Fluid Mech.* **165**, 163–199.

PERRY, A. E. & LI, J. D. 1990 Experimental support for the attached eddy hypothesis in zero-pressure-gradient turbulent boundary layers. *J. Fluid Mech.* **218**, 405–438.

PERRY, A. E., MARUSIC, I. & LI, J. D. 1994 Wall turbulence closure based on classical similarity laws and the attached eddy hypothesis. *Phys. Fluids* **2** (6), 1024–1035.

PIROZZOLI, SERGIO 2024 On the streamwise velocity variance in the near-wall region of turbulent flows. *Journal of Fluid Mechanics* **989**, A5.

PIROZZOLI, SERGIO, ROMERO, JOSHUA, FATICA, MASSIMILIANO, VERZICCO, ROBERTO & ORLANDI, PAOLO 2021 One-point statistics for turbulent pipe flow up to $re_\tau \approx 6000$. *Journal of Fluid Mechanics* **926**, A28.

SMITS, ALEXANDER J., HULTMARK, MARCUS, LEE, MYOUNGKYU, PIROZZOLI, SERGIO & WU, XIAOHUA 2021 Reynolds stress scaling in the near-wall region of wall-bounded flows. *Journal of Fluid Mechanics* **926**, A31.

TOWNSEND, A. A. 1976 *The Structure of Turbulent Shear Flow*. Cambridge University Press.

WEI, T., FIFE, P., KLEWICKI, J. C. & McMURTRY, P. 2005 Properties of the mean momentum balance in turbulent boundary layer, pipe and channel flows. *J. Fluid Mech.* **522**, 303–327.

WILCOX, D. C. 1995 *Perturbation Methods in the Computer Age*. DCW Industries, Inc.

YAMAMOTO, YOSHINOBU & TSUJI, YOSHIYUKI 2018 Numerical evidence of logarithmic regions in channel flow at $Re_\tau = 8000$. *Phys. Rev. Fluids* **3**, 012602.